

# Magnetorotational Instability in a Couette Flow of Plasma

Koichi Noguchi\* and Vladimir I. Pariev†

\*Applied Physics Division, Los Alamos National Laboratory, Los Alamos, NM 87545, USA

†Department of Physics and Astronomy, University of Rochester, Rochester, NY 14627, USA and  
Lebedev Physical Institute, Leninsky Prospect 53, Moscow 119991, Russia

**Abstract.** All experiments, which have been proposed so far to model the magnetorotational instability (MRI) in the laboratory, involve a Couette flow of liquid metals in a rotating annulus. All liquid metals have small magnetic Prandtl numbers,  $Pm \sim 10^{-6}$ , the ratio of kinematic viscosity to magnetic diffusivity. With plasmas both large and small  $Pm$  are achievable by varying the temperature and the density of plasma. Compressibility and fast rotation of the plasma result in radial stratification of the equilibrium plasma density. Evolution of perturbations in radially stratified viscous and resistive plasma permeated by an axial uniform magnetic field is considered. The differential rotation of the plasma is induced by the  $\mathbf{E} \times \mathbf{B}$  drift in applied radial electric field. Global unstable eigenmodes are calculated by our newly developed matrix code. The plasma is shown to be MRI unstable for parameters easily achievable in experimental setup.

## INTRODUCTION

A central problem in the theory of accretion disks in astrophysics is understanding the fundamental mechanism of angular momentum transfer. A robust anomalous outward angular momentum transport must operate in order for accretion to occur [1]. A phenomenological theory of turbulent angular momentum transport ( $\alpha$ -disks) proposed by Shakura [2] was in the basis of our understanding of how accretion occurs and still remains viable to date. The puzzle of the origin of turbulence in hydrodynamically stable disks was resolved when magnetorotational instability (MRI), originally discovered in Refs. [3] and [4], was applied to accretion disks by Balbus and Hawley [5]. MRI causes MHD turbulence to develop in an initially weakly magnetized fluid.

Despite its importance, MRI has never been observed in the laboratory. Recently, two experiments have been proposed to test MRI in a differentially rotating flow of liquid metal (Couette flow) between two rotating cylinders [6, 7]. A great deal of theoretical work on investigating MRI in Couette flow of liquid metals has been done confirming that MRI can be excited for magnetic Reynolds number,  $Rm$ , exceeding a few [8, 9, 10, 11]. A particular attention was given to why MRI was not observed in previous experiments with hydromagnetic Couette flows of liquid metals [8, 10]. Because of the very small magnetic Prandtl number of metals,  $Pm \sim 10^{-6}$ , the rotation needs to be very fast to achieve  $Rm > 1$ . Indeed, kinetic Reynolds number needs to exceed  $Re = Rm/Pm \sim 10^6$ . In previous experiments the rotation speed was not high enough to achieve  $Re \sim 10^6$ . For such high Reynolds numbers the flow in the experiment is likely to become turbulent even without a magnetic field for Rayleigh stable rotation

profiles. The instability may have a nonlinear hydrodynamic nature [12] or may be due to the Ekman circulation induced by the end plates [7]. The presence of such turbulence can affect the conditions for the excitation of MRI [7].

Here we consider plasma as alternative to liquid metals to use in MRI experiment. By changing temperature and density of the plasma by a few times around values  $T \sim 5 \text{ eV}$  and  $n \sim 10^{14} \text{ cm}^{-3}$  one can vary Pm in the range of about  $10^{-2}$  to  $10^2$ . For velocities of plasma of the order of the thermal speed of ions and the typical size of the apparatus of about 50cm Rm is in the range from  $10^2$  to  $10^3$ , while Re is in the range from 5 to  $10^4$ . These plasma parameters are readily achievable in the laboratory [13]. Therefore, in plasma experiment it can be relatively easy to have high enough Rm allowing for MRI to grow, while keeping Re modest and the flow laminar. Laminar character of the flow can allow a detailed study of the structure of the unstable mode and the secondary flow without intervening noise from turbulence. For higher Re  $\sim 10^4$ , the transition from laminar to turbulent flows in hydromagnetics can be investigated. Moreover, the effects of wide variations of Pm can be studied with a plasma MRI experiment.

## DESCRIPTION OF THE EXPERIMENT

The basic setup of possible plasma MRI experiment is illustrated in Fig. 1. This experiment is now under construction at Los Alamos National Laboratory. It can be also used for observing laminar plasma dynamos [13]. Tentative set of specifications and typical parameters of plasma for that experiment is shown in Table 1. The plasma is produced by the electric discharge in hydrogen and is injected into the space between two coaxial conducting cylinders. Mean free path for Coulomb collisions is much smaller than the radii of the cylinders, and MHD description of plasma is appropriate. Cylindrical coordinate system  $r, \phi, z$  is used with the axis of symmetry coinciding with the central axis of the cylinders. Axial uniform magnetic field  $B_{0z}$  is produced by the coils around the cylinders and is preexistent of the discharge. Therefore, plasma is coupled to the axial magnetic field lines already at the formation and can slide along the axial magnetic field lines filling the space between two cylinders. The outer cylinder is grounded and the voltage  $\Phi_0$  is applied to the inner cylinder during and after the plasma injection, in order to maintain the rotation. Neglecting the boundary and sheath modification of any applied electric field, plasma rotates with  $\mathbf{E} \times \mathbf{B}$  drift,

$$\mathbf{E}_0 = \frac{\Phi_0}{\ln(R_2/R_1)} \frac{1}{r} \mathbf{e}_r = -\frac{\mathbf{V}_0 \times \mathbf{B}_0}{c}, \quad (1)$$

where  $\mathbf{E}_0$  is the equilibrium electric field,  $\mathbf{B}_0 = B_{0z} \mathbf{e}_z$  is the equilibrium axial magnetic field,  $R_1$  is the radius of the inner cylinder,  $R_2$  is the radius of the outer cylinder, and  $c$  is the speed of light.

Since plasma is highly collisional and is thermalized before it reaches to the experimental region of the chamber, we further make an assumption that the stationary state is isothermal:

$$\Gamma P_0 / \rho_0 = C_s^2 = \text{constant}, \quad (2)$$

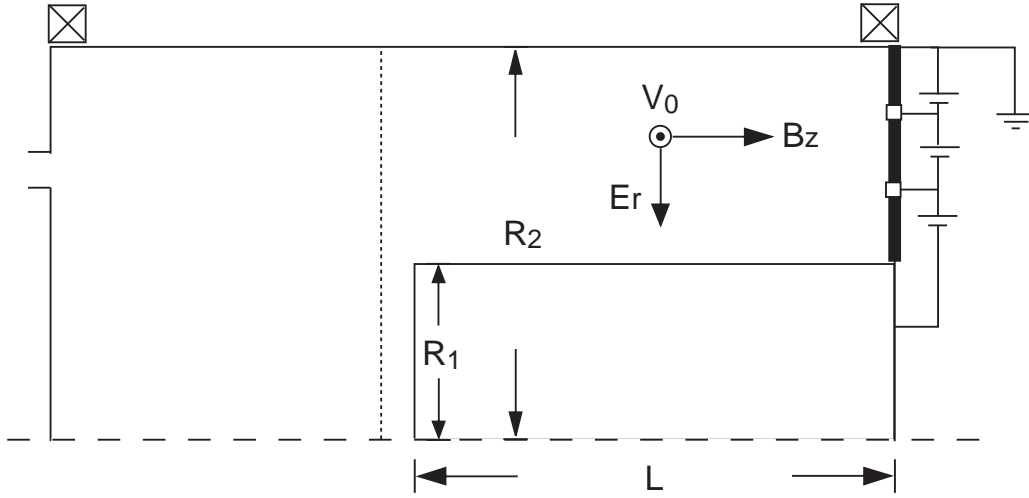


**FIGURE 1.** The meridional cross section of the device. Center line of the chamber is shown as a dashed line. Dotted line indicates the boundary of the working space between two cylinders (to the right). Plasma is injected from the left and rotates due to  $\mathbf{E} \times \mathbf{B}$  drift. Axial magnetic field is produced by coils. Coaxial metal rings at the right end plate are charged to fractions of  $\Phi_0$  ( $\Phi_0 < 0$  as illustrated) to support differential rotation of plasma against the formation of Ekman layer.

where  $P_0(r)$  is the equilibrium pressure,  $\rho_0(r)$  is the equilibrium density,  $C_s$  is the sound speed, and  $\Gamma$  is the ratio of specific heats ( $\Gamma = 5/3$  for hydrogen).

The Larmor radius of electrons in the experiment is also much smaller than the radii of the cylinders, but is comparable to the Coulomb mean free path. Despite this, here we assume for simplicity that the conductivity of the plasma is isotropic and is given by non-magnetized expression. The coefficient of magnetic diffusivity,  $\eta$ , and dynamic viscosity coefficient  $\rho\nu$  are independent of density and depends only on temperature. Then,  $\eta$  and  $\rho\nu$  remain constant throughout the volume of the plasma in the isothermal approximation considered here.

In the equilibrium state of the steady rotation the magnetic field is  $B_{0z} = \text{constant}$  and the velocity is  $\mathbf{V}_0 = (0, r\Omega(r), 0)$ , with the angular velocity profile

$$\Omega(r) = -\frac{\Phi_0}{B_{0z} \ln(R_2/R_1)} \frac{c}{r^2}. \quad (3)$$

Balance between the centrifugal force and the gradient of pressure in the equilibrium state is

$$-r\Omega^2\rho_0 = -\frac{dP_0}{dr}. \quad (4)$$

Using isothermal condition, Eq. (4) can be solved to give the radial dependence of  $\rho_0$

$$\rho_0 = \rho_0(R_1) \exp \left[ \int_{R_1}^r \frac{r\Gamma\Omega^2}{C_s^2} dr \right]. \quad (5)$$

When the rotation speed  $\Omega(R_1)R_1$  is comparable to the sound speed, the centrifugal force is significant enough to cause the compression of the plasma toward the outer cylinder.

**TABLE 1.** Parameters of the plasma.

Inner Radius $r_1$ (cm)	15
Outer Radius $r_2$ (cm)	52
Length $L$ (cm)	100
Density $n$ ( $\text{cm}^{-3}$ )	$1 \times 10^{14}$
Electron Temperature $T_e$ (eV)	5
Kinematic Viscosity, $\nu$ ( $\text{cm}^2 \text{s}^{-1}$ )	$3 \times 10^6$
Magnetic Diffusivity, $\eta$ ( $\text{cm}^2 \text{s}^{-1}$ )	$2.7 \times 10^5$
Prandtl number $P_m$	11
Sound Speed $C_s$ ( $\text{cm s}^{-1}$ )	$4 \times 10^6$
Maximum Frequency $\Omega_{1\text{max}}$ ( $\text{s}^{-1}$ )	$1.9 \times 10^5$

## THE INSTABILITY IN A RADIALLY STRATIFIED PLASMA

We consider perturbations of the equilibrium state described above:  $\mathbf{V} = \mathbf{V}_0 + \mathbf{v}$ ,  $\mathbf{B} = \mathbf{B}_0 + \mathbf{b}$ ,  $\rho = \rho_0 + \rho_1$ ,  $P = P_0 + P_1$ , and linearize MHD equations in small perturbations. We idealize the problem by considering cylinders of infinite length and take the dependence of perturbations on  $t$ ,  $\theta$ , and  $z$  as  $\propto \exp[i(-\omega t + m\theta + k_z z)]$ . If the equilibrium density  $\rho_0(r)$  varies significantly between  $R_1$  and  $R_2$ , general perturbations of the plasma are compressible. However, the phenomenon of MRI is due to the stretching of the magnetic field lines by the differential rotation coupled with the action of centrifugal force. Boussinesq approximation neglects the changes of the volume of the displaced parcel of plasma as it gets quickly adjusted to the new pressure equilibrium at a new radial location in the stratified plasma. It allows to capture centrifugal force acting on a displaced parcel of plasma but excludes compressible modes, which are not essential for the development of MRI. This simplifies calculations substantially. Here we adopt Boussinesq approximation. Linearized continuity equation becomes equivalent to two equations:

$$\frac{\partial \rho_1}{\partial t} + (\mathbf{V}_0 \nabla) \rho_1 + \mathbf{v} \cdot \nabla \rho_0 = 0, \quad (6)$$

$$\nabla \cdot \mathbf{v} = 0. \quad (7)$$

Other linearized MHD equations are:

$$\nabla \cdot \mathbf{b} = 0, \quad (8)$$

$$\frac{\partial \mathbf{b}}{\partial t} = \nabla \times (\mathbf{v} \times \mathbf{B}_0) + \nabla \times (\mathbf{V}_0 \times \mathbf{b}) + \eta \nabla^2 \mathbf{b}, \quad (9)$$

$$\begin{aligned} \rho_0 \frac{\partial \mathbf{v}}{\partial t} + \rho_0 (\mathbf{v} \nabla) \mathbf{V}_0 + \rho_0 (\mathbf{V}_0 \nabla) \mathbf{v} + \rho_1 (\mathbf{V}_0 \nabla) \mathbf{V}_0 = -\nabla P_1 + \rho_0 \nu_0 \nabla^2 \mathbf{v} \\ - \frac{1}{4\pi} \nabla (B_{0z} b_z) + \frac{1}{4\pi} (\mathbf{b} \nabla) \mathbf{B}_0 + \frac{1}{4\pi} (\mathbf{B}_0 \nabla) \mathbf{b}, \end{aligned} \quad (10)$$

where  $\nu_0$  is the unperturbed value of kinematic viscosity. Note, that  $\rho \nu = \rho_0 \nu_0$ , so that the viscosity coefficient  $\rho \nu$  remains unperturbed. The following reductions are done. First, we note that any solution of Eq. (9) satisfies Eq. (8) automatically. This means that out of four equations provided by (8) and (9) together, one should be omitted. We choose to omit  $z$ -component of Eq. (9) and use Eq. (8) to express  $b_z$  via  $b_r$  and  $b_\theta$  in

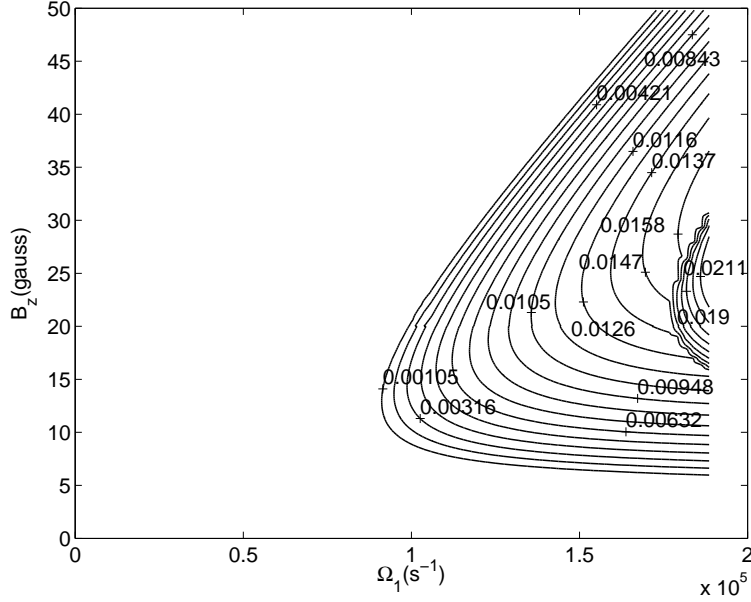


**FIGURE 2.** Growth rate,  $\text{Im } \omega / \Omega_1$ , of the unstable  $m = 0$ ,  $k_z = \pi/L$  mode as a function of  $\Omega_1$  and  $B_{0z}$

the  $r$  and  $\theta$  components of Eq. (9) as well as in all components of Eq. (10). We also use Eq. (7) to express  $v_z$  via  $v_r$  and  $v_\theta$ . Eq. (6) is used to express  $\rho_1$  via  $v_r$  and substitute into momentum Eq. (10). As for Eq. (10) we replace its  $z$ -component by the equation obtained by taking the divergence of Eq. (10). Using Eqs. (8) and (7) the divergence of Eq. (10) can be reduced to the equation with the only second order radial derivative being the  $\partial^2 \Pi / \partial r^2$ , where  $\Pi = P_1 + B_{0z} b_z / (4\pi)$  is the perturbation of the total pressure. In summary, we obtain five second order linear differential equations in  $r$  for five variables,  $\Pi$ ,  $b_r$ ,  $b_\theta$ ,  $v_r$ , and  $v_\theta$ : the divergence of Eq. (10),  $r$  and  $\theta$  components of induction Eq. (9), and  $r$  and  $\theta$  components of momentum Eq. (10)

An ideal conductor boundary is a good approximation, since  $\eta$  for metallic walls is  $< 800 \text{ cm}^2 \text{ s}^{-1}$ , which is always much smaller than that of plasma, so even a thin metallic wall can be considered as a good conductor. Boundary conditions for conducting walls are given by  $b_r = 0$ ,  $db_\theta/dr + b_\theta/r = 0$ ,  $v_r = 0$ ,  $v_\theta = 0$ ,  $dv_r/dr = 0$  at both  $r = R_1$  and  $R_2$ .

We discretize the equations and boundary conditions on a uniform grid in rescaled variable  $x = \ln(r/R_1)$  with  $N = 200$  grid points. The problem is reduced to finding values of  $\omega$  such that the determinant of the matrix  $5N \times 5N$  is zero. We calculate the determinant by using LU-decomposition and search for zeros by using Newton iteration method. After an eigenvalue of  $\omega$  is found, the corresponding eigenfunction is calculated by using back substitution.

We find  $m = 0$  axisymmetric unstable mode in a wide range of parameters achievable in the experiment. Let us focus on one case with fixed temperature and density given in Table 1. Then,  $C_s(T)$  and  $\text{Pm}(\rho, T)$  are also fixed. The remaining parameters, which can be adjusted in the experiment, are  $\Phi_0$  and  $B_{0z}$ . For angular velocity profile (3) the value of  $\Phi_0$  is uniquely related to the value of  $\Omega_1 = \Omega(R_1)$ . The velocity of the

plasma should be subsonic everywhere for Boussinesq approximation to be a reasonable approximation. At supersonic speeds, plasma is pushed close to the outer wall leaving very rarefied region in the bulk between cylinders. In this case, it is more appropriate to discuss buoyant or Parker instabilities than MRI. The velocity of rotation is maximum near the inner cylinder, therefore, our calculations are valid for  $\Omega_1 R_1 < C_s$ . The maximum value  $\Omega_{1\max} = C_s/R_1$  is given in Table 1.

We plotted the MRI growth rate  $\text{Im}(\omega)/\Omega_1$  for  $m = 0$ ,  $k_z = \pi/L$  mode in Fig. 2. We also searched for the unstable non-axisymmetric modes, but did not find any. In a small region to the right in Fig. 2 with small contour separation the mode is purely growing ( $\text{Re}(\omega) = 0$ ), in the rest of the unstable region the mode is growing and oscillating ( $\text{Re}(\omega) > 0$ ). The MRI is absent for weak magnetic fields ( $v_{Az}/C_s \ll 10^{-2}$ ) and small wave numbers ( $k_z L < 2\pi$ ) because driving force from magnetic field is too weak to overcome the viscosity and diffusivity. The MRI is also suppressed in high magnetic field region due to magnetic tension. For a given magnetic field, only finite number of modes in the  $k_z$  direction will be excited.

The drawback of using plasmas is limited time available before plasma recombines enough to significantly reduce its coupling with the magnetic field. During the confinement time of the order of  $10^{-3}$  s initial perturbations grow by  $\sim 10$  times, and can be registered experimentally. This confinement time is within the range of planned experiment.

## ACKNOWLEDGMENTS

The authors are grateful to Zhehui Wang of Los Alamos National Laboratory for encouraging the present work and support. Discussions with Hantao Ji and Jeremy Goodman were very useful. KN acknowledges support from DOE through the LDRD-ER program at Los Alamos National Laboratory. VP acknowledges support from DOE grant DE-FG02-00ER54600.

## REFERENCES

1. Frank, J., King, A., and Raine, D.J., *Accretion Power in Astrophysics: Third Edition*, Cambridge University Press, Cambridge, 2002.
2. Shakura, N.I., *Astron. Zhurnal* **49**, 921-929 (1972).
3. Velikhov, E.P., *J. Exptl. Theoret. Phys.* **36**, 1398-1404 (1959).
4. Chandrasekhar, S., *Proc. Natl. Acad. Sci.* **46**, 253-257 (1960).
5. Balbus, S.A., and Hawley, J.F., *Astrophys. J.* **376**, 214-233 (1991).
6. Ji, H., Goodman, J., and Kageyama, A., *Mon. Not. Roy. Astron. Soc.* **325**, L1-L5 (2001).
7. Noguchi, K., Pariev, V.I., Colgate S.A., Nordhaus J., and Beckley H.F., *Astrophys. J.* **575**, 1151-1162 (2002).
8. Goodman, J., and Ji, H., *J. Fluid Mech.* **462**, 365-382 (2002).
9. Rüdiger, G., and Zhang, Y., *Astron. Astrophys.* **378**, 302-308 (2001).
10. Rüdiger, G., Schultz, M., and Shalybkov, D., *Phys. Rev. E* **67**, 046312 (2003).
11. Willis, A.P., and Barenghi, C.F., *Astron. Astroph.* **388**, 688-691 (2002).
12. Richard, D., and Zahn, J.-P., *Astron. Astroph.* **347**, 734-738 (1999).
13. Wang, Z., Pariev, V.I., Barnes, C.W., and Barnes, D.C., *Phys. Plasmas* **9**, 1491-1494 (2002).